# STUDY ON THE DYNAMICS OF KAMAZ 43118 VEHICLE OPERATING UNDER LATERAL FORCE EFFECTS

**Bui Van Hai[1], Nguyen Phi Truong[1,*], Nguyen Ngoc Anh[2]**

DOI: https://doi.org/10.57001/huih5804.2026.015

**ABSTRACT**

This study analyses the dynamic characteristics of the KAMAZ 43118 off-road truck under lateral forces, which are critical for vehicle stability and driving safety. Employing a multi-degree-of-freedom vehicle dynamics model, the equations of motion were derived, incorporating the effects of crosswind and steering angle. Simulations were performed in MATLAB/Simulink to analyse the variations of essential factors such as lateral velocity, lateral acceleration, sideslip angle, and yaw rate. This research investigates the influence of crosswind pressures and steering manoeuvres on vehicle stability through dynamic simulations. Results demonstrate that under crosswind forces of 100 - 1000N, lateral displacement increases from several centimetres to over 0.2m, while the yaw angle rises to around 0.05°, indicating a notable deviation from the intended path. During lane-change movements with steering inputs of ±1°, the vehicle exhibits a maximum lateral displacement of 1.6 - 1.7m and a peak yaw angle of around 0.048°. Augmented lateral forces amplify both displacement and yaw response, highlighting the elevated risk of instability at higher velocities. The findings underscore the critical significance of steering dynamics, suspension, and tyre performance in maintaining stability, and suggest the necessity for advanced active control systems to improve vehicle safety in adverse situations.

***Keywords:*** *Crosswind aerodynamics, yaw moment, lateral stability.*

[1]School of Mechanical and Automotive Engineering Hanoi University of Industry, Vietnam

[2]Center for Automobile Technology and Driving Training, Hanoi University of Industry, Vietnam

[*]Email: truongnp@haui.edu.vn

Received: 02/10/2025

Revised: 15/01/2026

Accepted: 28/01/2026

## 1. INTRODUCTION

The dynamics of the KAMAZ 43118 vehicle under lateral loads involve several factors, including vehicle stability, suspension performance, and operating safety (Figure 1). The current literature elucidates the behavior of heavy-duty vehicles under lateral forces, highlighting the significance of suspension components and vehicle design in preserving stability. Recent advancements in vehicle suspension systems indicate that improved shock absorbers are essential for controlling lateral forces in trucks such as the KAMAZ 43118. The KAMAZ absorber, an essential element of the suspension system, is engineered to attenuate shocks and reduce the effects of lateral forces during operation, hence improving vehicle stability and ride comfort [1]. This corresponds with the comprehensive recognition that efficient suspension systems are crucial for large vehicles functioning under dynamic lateral forces. Moreover, the significance of vehicle components, including support bearings and constant velocity (CV) joints, is emphasized in enhancing vehicle dynamics under diverse operating angles and lateral loads. These components facilitate the adjustment of operational fluctuations, mitigating the detrimental impacts of lateral loads and enhancing handling smoothness and safety margins [2]. Although there are no particular studies on the KAMAZ 43118 concerning lateral force impacts, similar research on other heavy vehicles indicates that the interplay between vehicle construction and external lateral forces considerably affects operational safety. The examination of metro train dynamics over curved bridges with resilient wheels highlights the significance of coupled dynamic models in comprehending vehicle responses to lateral stresses in intricate settings [3]. These models could be modified to assess the KAMAZ 43118's performance under lateral loads, taking into account its distinctive structural and suspension attributes. The acknowledgment of vehicle stability in operational scenarios, including collision avoidance systems and vehicle safety evaluations, highlights the importance of comprehending lateral force dynamics. Advanced techniques for vehicle-to-vehicle (V2V) and vehicle-to-

pedestrian (V2P) accident prevention are being developed to reduce risks linked to lateral movements and external forces. These technological innovations are essential for the functioning of heavy-duty vehicles in demanding environments characterized by significant lateral forces. The present study demonstrates that the stability and safe operation of the KAMAZ 43118 under lateral forces are significantly influenced by suspension components, such as shock absorbers and support bearings, in addition to the vehicle's structural design. The incorporation of dynamic modeling techniques, such to those employed in train and bridge interaction studies, may improve comprehension and management of lateral force effects on heavy vehicles. These insights are essential for enhancing vehicle design, operating safety, and performance in situations characterized by substantial lateral forces [1, 2, 4, 5]. This study presents specific examples that augment existing research on the influence of lateral force factors on the stability of moving vehicles.

Figure 1. The Kamaz 43118

## 2. VEHICLE DYNAMICS MODEL UNDER LATERAL FORCE

Examine the dynamic model illustrated in Figure 2. The model possesses three degrees of freedom: longitudinal displacement (x), lateral displacement (y), and yaw angle (ψ) on the vertical axis that intersects the vehicle's centre of gravity (CG). The coordinate system XCY is affixed to the centre of gravity (CG). The steering wheels are rotated by an angle δ, while the front and rear wheels exhibit slip angles $\alpha_i$ (i = 4). At the tire-road contact patch, the longitudinal and lateral forces are denoted as $F_{xf}$, $F_{yf}$, $F_{xr}$, and $F_{yr}$. At the centre of gravity, inertia forces exert influence in the longitudinal direction ($m_{vx}$), lateral direction ($m_{vy}$), and by centrifugal force, $m_v\ddot{\Psi}\sqrt{x^2+\dot{y}^2}$, in addition to the yaw moment of inertia $J_v\ddot{\Psi}$. Utilising D'Alembert's principle results in a series of differential equations that characterise the dynamics during the vehicle's directional change. In the typical scenario of crosswind loading, tyre forces are presumed to exert influence at the contact patches, disregarding rolling resistance and assuming a symmetric static load distribution [6].

Considering equilibrium along the x-direction:

$$\begin{aligned}&-m_v\dot{v}_x+m_v v_y(\dot{\psi}+\dot{\beta})+F_{x1}\cos\delta_1+F_{x2}\cos\delta_2+F_{x3}+F_{x4}\\&-F_{y1}\sin\delta_1-F_{y2}\sin\delta_2-F_w=0\end{aligned} \quad (1)$$

Considering equilibrium along the y-direction:

$$\begin{aligned}&-m_v\dot{v}_y+m_v v_x(\dot{\psi}+\dot{\beta})+F_{x1}\sin\delta_1+F_{x2}\sin\delta_2+F_{y1}\cos\delta_1\\&+F_{y2}\cos\delta_2+F_{y3}+F_{y4}+N=0\end{aligned} \quad (2)$$

The moment equation with respect to the vehicle's center of gravity is determined as follows:

$$\begin{aligned}&-J_v\ddot{\psi}+F_{y1}\cos\delta_1.L_f+F_{y2}\cos\delta_2.L_f-F_{y3}.L_r-F_{y4}.L_r\\&+F_{y1}\sin\delta_1.T_r-F_{y2}\sin\delta_2.T_f+F_{x1}\sin\delta_1.L_f+F_{x2}\sin\delta_2.L_f\\&-F_{x1}\cos\delta_1.T_r+F_{x2}\cos\delta_2.T_f-F_{x3}.T_r+F_{x4}.T_r+N.l_a=0\end{aligned} \quad (3)$$

Considering the two-track model while neglecting longitudinal dynamics, assuming the vehicle moves at a constant speed $\dot{x}=v_0$, with $F_{x1}=F_{x2}=F_{x3}=F_{x4}=0$, and the vehicle body sideslip angle β being negligible. The steady-state cornering dynamic model can be rewritten as follows

$$\dot{v}_y=-\dot{v}_x\dot{\psi}+\frac{1}{m_v}\left[F_{y1}\cos\delta_1+F_{y2}\cos\delta_2+F_{y3}+F_{y4}+N\right] \quad (4)$$

$$\begin{aligned}&\ddot{\psi}=\frac{1}{J_v}[F_{y1}\cos\delta_1.L_f+F_{y2}\cos\delta_2.L_f-F_{y3}.L_r-F_{y4}.L_r\\&+F_{y1}\sin\delta_1.T_r-F_{y2}\sin\delta_2.T_f+N.l_a]\end{aligned} \quad (5)$$

Considering the linear model:

$$F_{y1}=F_{y2}=C_f\alpha_f, F_{y3}=F_{y4}=C_r\alpha_r \quad (6)$$

The slip angles of the front and rear wheels are determined as follows:

Front wheels:

$$\alpha_f=\delta_1-\arctan\left(\frac{L_f\dot{\psi}+\dot{y}}{\dot{x}}\right)\approx\delta_1-\frac{L_f\dot{\psi}+\dot{y}}{v_0} \quad (7)$$

Rear wheels: $$\alpha_r=-\arctan\left(\frac{-L_r\dot{\psi}+\dot{y}}{\dot{x}}\right)\approx\delta_1-\frac{L_r\dot{\psi}+\dot{y}}{v_0} \quad (8)$$

$$\begin{aligned}&\Leftrightarrow F_{y1}=F_{y2}=c_f.\left(\delta_1-\frac{L_f\dot{\psi}+\dot{y}}{v_0}\right);\\&F_{y3}=F_{y4}=c_r.\left(\frac{L_r\dot{\psi}+\dot{y}}{v_0}\right)\end{aligned} \quad (9)$$

Substituting (9) into (4) and transforming (5), we obtain:

$$\Leftrightarrow \dot{v}_y = -\frac{c_f\cos\delta_1 + c_f\cos\delta_2 + 2c_r}{m_v v_0}\dot{y} + \left[\frac{2.c_rL_r - c_fL_f\cos\delta_1 - c_fL_f\cos\delta_2}{m_v v_0} - v_0\right]\dot{\psi} + \frac{\delta_1 c_f\cos\delta_1}{m_v} + \frac{\delta_2 c_f\cos\delta_2}{m_v} + \frac{N}{v_0} \quad (10)$$

$$\ddot{\psi} = \frac{c_fL_f^2\cos\delta_1 - c_fL_f^2\cos\delta_2 - 2c_rL_r^2 - c_fL_fT_r\sin\delta_1 + c_fL_fT_f\sin\delta_2}{J_v v_0}\dot{\psi} + \frac{2c_rL_r - c_fL_f\cos\delta_1 - c_fL_f\cos\delta_2 - c_fT_r\sin\delta_1 + c_fT_f\sin\delta_2}{J_v v_0}\dot{y} + \frac{c_f\delta_1L_f\cos\delta_1 + c_f\delta_2L_f\cos\delta_2 + c_f\delta_1T_r\sin\delta_1 - c_f\delta_2T_f\sin\delta_2}{J_v} + \frac{Nl_a}{J_v} \quad (11)$$

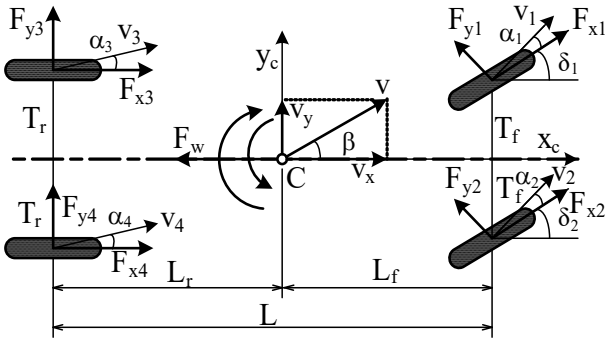


Figure 2. Dynamic model of vehicle motion [1]

## 3. DEVELOPMENT OF A SIMULATION MODEL USING MATLAB-SIMULINK AND DISCUSSION

### 3.1. Simulation input parameters

A simulation model of vehicle dynamic motion is constructed using MATLAB/Simulink. The model comprises a block for vehicle body dynamics and a block for converting from the moving coordinate system at the vehicle's centre of gravity to the fixed coordinate system affixed to the road. The inputs to the vehicle body dynamics module comprise lateral wind force and the steering wheel angle of the front wheels (Table 1).

Table 1. Input parameters [6]

| Technical Parameter | Kamaz 43114 Vehicle |
|---|---|
| $m_v$: Vehicle mass (kg) | 10850 |
| $L_f$: Distance from CG to front axle wheel track center (m) | 4.2 |
| $L_r$: Distance from CG to rear axle wheel track center (m) | 5.35 |
| $l_a$: Distance from CG to lateral load application point (m) | 2 |
| $C_f$: Cornering stiffness coefficient, front axle | 6.370×2.405×600 |
| $C_r$: Cornering stiffness coefficient, rear axle | 4.420×1.300 |
| $T_f, T_r$: Half track width of front and rear axles | 2.505/2 |
| Steering angle (rad) | $\delta_1, \delta_2$ = 0.261799 rad = 15 degrees or 0.436332 rad = 25 degrees |
| $v_0$: Vehicle speed under study (km/h) | 30 |
| $J_v$: Moment of inertia about vertical axis through vehicle CG (kg.m$^2$) | $m_vL_fL_r$= 2.437995e+05 |

### 3.2. Simulation of vehicle trajectory during straight-line drive with a constant steering angle (δ = 0) under lateral force

A vehicle model travelling in a straight line with a steering angle of (δ = 0) experiences a sudden lateral wind force while driving at a speed of 30 km/h for a duration of 10 seconds. Figure 3 depicts the lateral wind force exerted on the vehicle during the experiment, showcasing various force magnitudes.

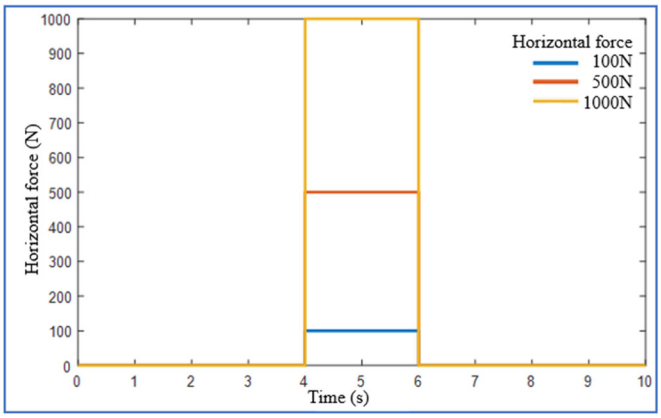


Figure 3. Lateral wind N acting on the vehicle during the simulation

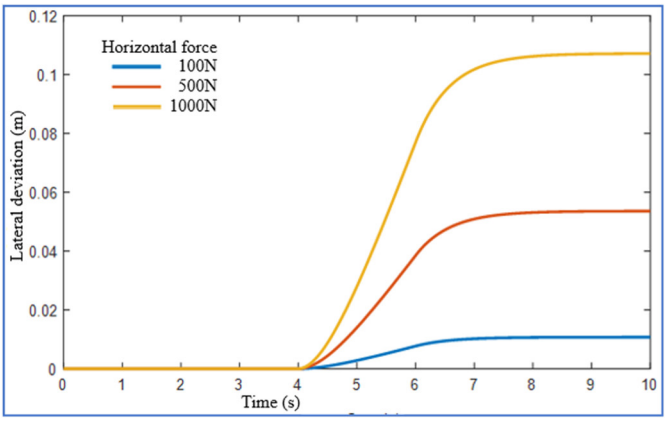


Figure 4. Lateral displacement with a steering angle of 0 degrees

The input parameters are applied during the simulation period from 4 seconds to 6 seconds. The

vehicle encounters lateral wind forces of 100N, 500N, and 1000N, applied 2m posterior to its centre of gravity. Figure 5 depicts the course of the vehicle.

Figures 3 ÷ 6 illustrate that crosswind forces (100 - 1000N) cause lateral displacement and yaw angle, especially noticeable between 4 - 6s. The maximum lateral displacement reaches about 0.11m and the yaw angle about 0.11° under a 1000N crosswind. After the wind subsides, the vehicle remains offset and cannot self-stabilize effectively. Therefore, corrective steering action (Figure 6) is required to return the vehicle to a safe trajectory.

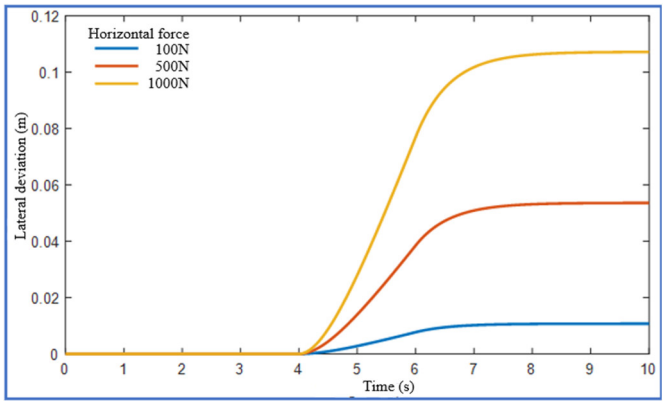


Figure 5. Vehicle yaw angle (ψ) under the effect of a sudden lateral wind with a steering angle of 0 degrees

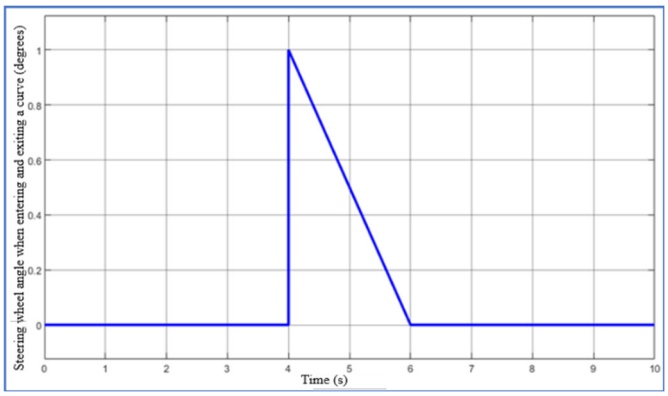


Figure 6. Steering wheel angle during corner entry and exit

### 3.3. Simulation of the vehicle's trajectory during corner entry and exit at a cornering angle of 25 degrees

Simulation of the vehicle's trajectory during cornering. The steering wheel angle progressively elevates in one direction before reverting to the straight-driving position. Figure 7 illustrates the fluctuation of the steering wheel angle during corner entry and departure. The driver maintains the steering wheel in a straight position during the initial 4 seconds of the simulation, then steering in one direction at a pace of 100°/s until reaching 250°, before reversing the wheel in the opposite direction at the same rate. Specifically, in the first 6 - 7 seconds, the curves rise rapidly and then converge to a stable value (3.45 - 3.55m), reflecting the vehicle's cornering process and dynamic equilibrium. The greater the trajectory deviation, the more it indicates understeer, especially at high lateral force (1000N), which can easily cause instability and side slip. Figure 8 depicts the vehicle's lateral displacement during corner entry and exit. At 4 seconds, the vehicle initiates a change in its travel direction, accompanied by a diminishing turning radius. Subsequently, the steering wheel angle progressively reverts to 0°, the turning radius expands, and by 6 seconds, the vehicle resumes linear motion. Specifically, as the lateral force escalates (100 → 1000N), the car's yaw angle correspondingly increases, demonstrating that a greater lateral force induces a more pronounced rotation of the vehicle in relation to the steering input. The disparities across the curves are negligible (about 0.005 - 0.01°), suggesting that the suspension and tyres continue to uphold stability within this force range. At 1000N, the yaw angle significantly increases, indicating a potential risk of moderate oversteer, wherein the vehicle's rear may pivot outward once the lateral force beyond the tyre adhesion threshold.

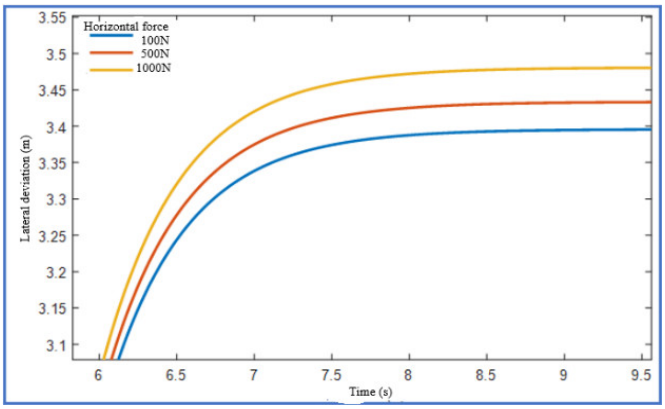


Figure 7. Vehicle trajectory during corner entry and exit

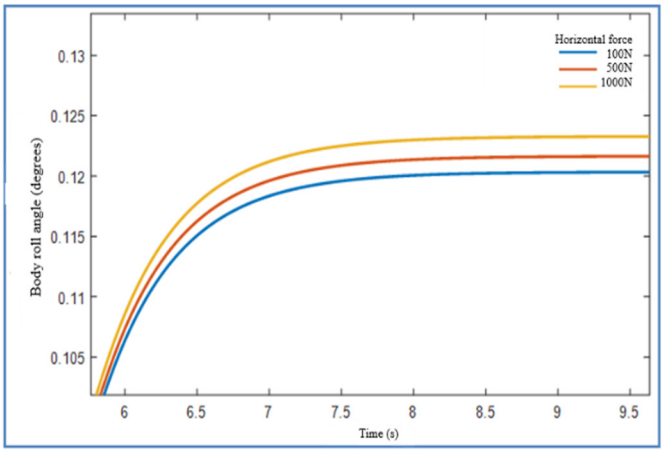


Figure 8. Vehicle yaw angle during corner entry and exit

### 3.4. Simulation of the vehicle's trajectory during corner entry and exit at a cornering angle of 25 degrees

Figure 9 illustrates that from 0 to 4 seconds, the steering angle remains at 0°, signifying linear motion. Between 4 and 5.5 seconds, the steering angle exhibits a positive increase of around +1°, indicating a right turn. It thereafter declines sharply to a negative value (≈ –1°), indicating a left turn. After 6 seconds, the steering angle reverts to 0°, and the vehicle achieves stabilisation in linear motion.

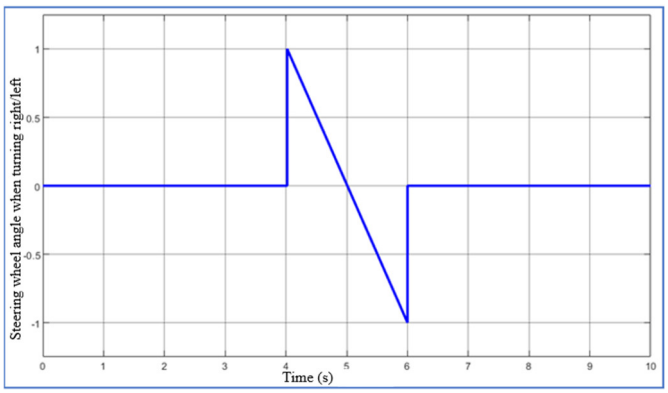


Figure 9. Steering wheel angle during right and left cornering

Figure 10 illustrates that from 0 to 4 seconds, the lateral displacement is approximately zero, signifying linear motion. Between 4 and 6 seconds, the displacement rises significantly, to a maximum of approximately 1.6 to 1.7 metres, indicative of the lane-change manoeuvre. After 6 seconds, the displacement progressively diminishes and stabilises close to zero as the vehicle reverts to its previous trajectory. As lateral force increases from 100 to 1000N, the peak displacement exhibits a modest increase, indicating that more lateral force results in larger departures from the optimal trajectory.

Figure 9 illustrates the driving maneuvers of "turn right - turn left - turn straight" at intervals of 4 - 6 seconds. Figure 10 illustrates a marked horizontal deviation during this period, peaking at about 1.6 - 1.7m, then stabilizing near 0. An increase in horizontal force results in more vehicle deflection, signifying a heightened danger of instability during high-speed lane changes.

Figure 11 illustrates that the yaw angle maintains almost zero from 0 to 4 seconds, subsequently increasing abruptly to approximately 0.046 - 0.048° between 4 and 6 seconds, indicating the vehicle's response to steering input. Subsequent to 6 seconds, it diminishes and stabilises at 0.005 - 0.01°. While a greater lateral force (1000N) results in a little elevated peak, the disparity is insignificant, suggesting that the suspension and tyres uphold stability within this range.

In conclusion, Figures 9 ÷ 11 distinctly demonstrate the correlation among steering angle, lateral displacement, and yaw angle. Between 4 and 6 seconds, steering input produces a peak lateral displacement of around 1.6 to 1.7 metres and a maximum yaw angle of about 0.048 degrees. Elevated lateral forces exacerbate these responses, signifying a heightened danger of instability during high-velocity lane-change manoeuvres.

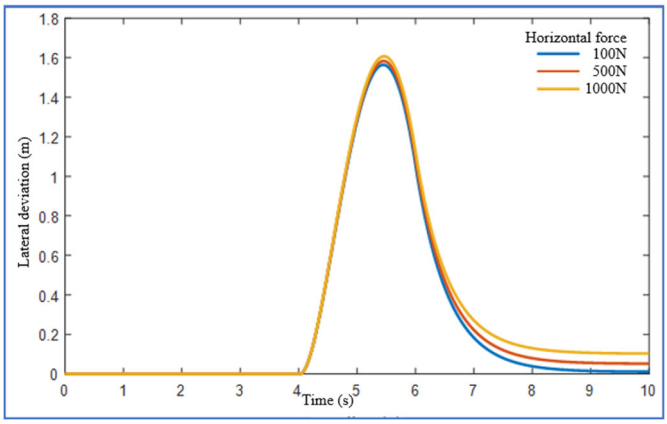


Figure 10. Vehicle trajectory during right and left turning

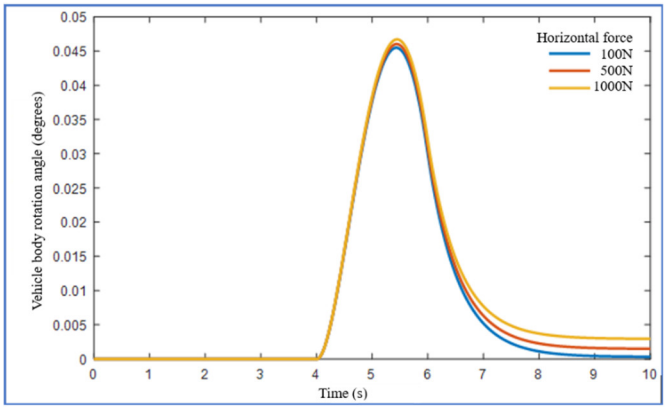


Figure 11. Vehicle yaw angle during right and left turning

## 4. CONCLUSION

The simulation results indicate that crosswind forces and steering manoeuvres substantially influence vehicle stability. Under crosswind forces of 100 - 1000N (Figures 3 ÷ 5), the lateral displacement escalated from few centimetres to over 0.2m, while the yaw angle attained around 0.05°, signifying a significant divergence from the intended path. In lane-change manoeuvres (Figures 6 ÷ 11), a steering input of ±1° produced a peak lateral displacement of approximately 1.6 - 1.7m and a maximum yaw angle of ~0.048°. Elevated lateral forces intensified both displacement and yaw reaction, underscoring the heightened risk of instability,

particularly at elevated velocities. The study highlights the essential importance of steering dynamics, suspension, and tyre attributes in preserving stability, while also stressing the need for sophisticated active control systems to improve vehicle safety.

**REFERENCES**

[1]. Kamaz. (n.d.), *Absorber - High quality shock absorbers for trucks 1*. Retrieved from https://www.kamaz.ru/

[2]. Cardriveshafts. (n.d.). *Support bearing*. Retrieved from https://www.cardriveshafts.com/.

[3]. Wu Y., Pu Q., Chen Z., Hong X., Wang X., "Dynamic characteristics and safe operation speed threshold of metro train passing through curved bridge considering resilient wheel," *Scientific Reports*, 2025. https://doi.org/10.1038/s41598-025-XXXXX

[4]. Xi X., Xiao J., Zhang Q., Wang Y., "Pavement state recognition method considering slope," *Journal of Physics: Conference Series,* 1885(1), 012345, 2021. https://doi.org/10.1088/1742-6596/1885/1/012345

[5]. Zyfra. (n.d.), *Zyfra examines advanced systems for V2V, V2P collision avoidance*. Retrieved from https://www.zyfra.com/

[6]. Vasina V. V. (n.d.), *Kamaz automobiles*. Department of Development and Implementation of New Developments, Republic of Tatarstan, Russia.

[7]. Mastinu M., Gobbi M., Pavesi G., *Vehicle dynamics: Theory and applications*. Cham, Switzerland: Springer, 2022. https://doi.org/10.1007/978-3-030-95251-0

[8]. Ehlers S. F. G., Ziaukas Z., Kobler J. P., Busch A., Ortmaier T., Wielitzka M., "Nonlinear two-track model of a semitrailer with experimental validation of lateral and vertical tire forces," *arXiv preprint* arXiv:2407.10270, 2024. https://arxiv.org/abs/2407.10270